water

MDPI

Article

Contrasting Dissolved Organic Carbon Cycling in Open and Closed Karst Reservoirs Water: Evidence from Dual Carbon Isotopes ($\delta^{13}C$–$\Delta^{14}C$)

Xia Yu [1,2,*,†], Hao Liu [2,3,†], Bingyang Dai [1], Xuran Liu [1], Zilin Mei [1], Chao Ma [1], Chengzhi Yang [1], Mingyu Shao [2] and Yanling An [1]

[1] College of Resources and Environmental Engineering, Guizhou Institute of Technology, Guiyang 550003, China
[2] State Key Laboratory of Environmental Geochemistry, Institute of Geochemistry, Chinese Academy of Sciences, Guiyang 550001, China
[3] College of Resources and Environment, University of Chinese Academy of Sciences, Beijing 100049, China
* Correspondence: yuxia@git.edu.cn
† These authors contributed equally to this work.

Abstract

Reservoirs in karst regions exhibit significant carbon sink potential; however, how different reservoir types influence carbon sequestration remains poorly understood. In this study, dual carbon isotopes ($\delta^{13}C$–$\Delta^{14}C$) were applied to trace dissolved organic carbon (DOC) sources in an open reservoir (Aha Reservoir, AHR) and a closed reservoir (Guanshan Lake, GSL) in southwestern China, and to evaluate their carbon sequestration potential. DOC concentrations in GSL were significantly higher than those in AHR (4.14 ± 0.28 mg/L > 3.37 ± 0.30 mg/L) ($p < 0.01$), along with lower $\delta^{13}C$ values (-30.34 ± 0.51‰ < -28.18 ± 0.31‰) and more enriched $\Delta^{14}C$ values (-6.94 ± 11.07‰ > -93.74 ± 6.76‰). The $\delta^{13}C$–$\Delta^{14}C$ tracing revealed that plants were the primary DOC source for AHR (61 ± 2%), whereas algae dominated DOC sources in GSL (70 ± 2%). Inflow rivers and water retention time (WRT) likely drive differences in DOC sources and concentrations between the two reservoirs. The absence of inflow rivers and the longer WRT in GSL created favorable conditions for algal growth, resulting in substantially higher chlorophyll a (Chl.a) concentrations (103.00 ± 29.87 μg/L > 13.10 ± 3.29 μg/L) and enhanced production of autochthonous DOC through a stronger biological carbon pump (BCP) effect. These conditions further facilitate the formation and accumulation of recalcitrant DOC (RDOC), ultimately increasing DOC concentrations in GSL. Our findings highlight that closed karst reservoirs may represent important yet underappreciated carbon sinks and should receive greater attention in future carbon-sink assessments.

Keywords: DOC; $\delta^{13}C$–$\Delta^{14}C$; open-reservoir; closed-reservoir; transformation

Check for updates

Academic Editor: Juan José Durán

Received: 10 May 2026
Revised: 6 June 2026
Accepted: 8 June 2026
Published: 16 June 2026

Copyright: © 2026 by the authors. Licensee MDPI, Basel, Switzerland. This article is an open access article distributed under the terms and conditions of the Creative Commons Attribution (CC BY) license.

1. Introduction

Dissolved organic carbon (DOC) is the predominant fraction of aquatic organic carbon, accounting for approximately 80% of total organic carbon [1,2]. It serves as a key indicator of organic matter content and biological activity in water bodies [3], playing a pivotal role in the biogeochemical cycles of aquatic ecosystems [4,5]. Terrestrial organic carbon transported by rivers leads to the burial of approximately 60 Tg of organic carbon annually in global reservoirs, accounting for about 40% of global organic carbon storage [6]. Consequently, investigating the transport, transformation, and geochemical behavior of DOC in

inland reservoirs is crucial for enhancing carbon sequestration in aquatic carbon pools and addressing climate change [7,8]. DOC originates from two primary sources: autochthonous (phytoplankton derivatives) and allochthonous (from soil erosion and anthropogenic activities) [9]. Autochthonous DOC is mainly produced by algae and aquatic macrophytes, while allochthonous DOC is primarily transported via rivers and significantly influenced by soil organic matter, wastewater discharge, and plant debris [10,11]. DOC undergoes three principal fates: (1) release into the atmosphere through microbial mineralization and respiration; (2) photodegradation, which primarily affects terrestrially derived organic compounds; and (3) mineral adsorption, subsequently stored in sediments as particulate organic carbon (POC) [2,8,12,13].

China hosts one of the world's largest karst regions, which is mainly distributed in southwestern China, where numerous reservoirs have been constructed in recent decades [14]. The high solubility and rapid weathering kinetics of carbonate rocks in karst regions consume substantial atmospheric CO_2, resulting in dissolved inorganic carbon (DIC) concentrations 6–10 times higher than those in non-karst areas [15,16]. While elevated DIC concentrations could potentially be re-emitted to the atmosphere through air-water exchange and calcium carbonate formation, karst reservoirs paradoxically demonstrate lower CO_2 emissions compared to their non-karst counterparts [17]. This phenomenon mainly results from the conversion of DIC into autochthonous organic carbon (AOC) via aquatic photosynthesis (the biological carbon pump, BCP), followed by long-term burial [18–21]. These findings suggest that karst reservoirs function as effective carbon sinks.

Isotopes, as effective tracers, have been consistently employed in studies of carbon cycling in water bodies in karst landscapes. For example, $\delta^{13}C$ was used to analyze the impact of dam construction in the Three Gorges Reservoir on the geochemical behavior of DIC [22]. However, the relatively narrow range of $\delta^{13}C$ values in organic carbon (−32‰ to −12‰) often leads to overlapping source end-members, leading to potential inaccuracies in data interpretation [23]. With recent advances in accelerator mass spectrometry (AMS), $\Delta^{14}C$ values offer a broader range and higher resolution (−1000‰ to 200‰). For example, Chen et al. [24] used dual carbon isotopes ($\delta^{13}C$–$\Delta^{14}C$) to trace the sources of POC in Fuxian Lake in a karst region and found that the contribution rate of endogenous aquatic photosynthesis was 61%. Meanwhile, Qiu et al. [25] used $\delta^{13}C$–$\Delta^{14}C$ to find that rivers contributed as much as 70% of the DIC in AHR. In addition, Liu et al. [26] used $\delta^{13}C$–$\Delta^{14}C$ to discover that karst regions have a strong BCP effect, and that aquatic plants utilize organic carbon converted from DIC with a negative $\Delta^{14}C$ value.

Distinct carbon-cycling patterns are often observed among different types of reservoirs. For instance, the Wulihe Reservoir on the Loess Plateau, characterized by longer water retention time (WRT), exhibits a more pronounced BCP effect and lower CO_2 emissions compared to the Honghe Reservoir with relatively shorter WRT [27]. Concurrently, Liu et al. [28] reported that DIC in closed reservoirs typically displays more positive $\Delta^{14}C$ values than in open reservoirs. This indicates that DIC exhibits distinct geochemical behaviors among reservoirs with different hydrological characteristics. However, in previous studies, AOC converted by the BCP was mostly calculated based on POC, while the contribution of DOC to AOC was ignored [1]. Moreover, analytical challenges and molecular complexity of DOC have resulted in significantly less understanding compared to inorganic carbon [29–31]. Despite recent progress in DOC research, such as the finding that DOC sources in the Lijiang River vary across seasons and locations [32], significant knowledge gaps remain regarding the transport and transformation of DOC in reservoirs with different hydrological characteristics in karst regions. To advance our understanding of DOC geochemistry in karst reservoirs, this study employs $\delta^{13}C$–$\Delta^{14}C$ analysis to compare open and closed reservoirs, aiming to reveal DOC sources and their migration and transformation

processes, and differences in their carbon sequestration potential. The objectives of this study are as follows: (1) to quantify DOC sources using $\delta^{13}C$–$\Delta^{14}C$; (2) to reveal DOC cycling processes and stabilization mechanisms; (3) to identify the differences in DOC geochemical behavior between open and closed reservoirs and their underlying causes.

2. Materials and Methods

2.1. Study Area

The study area is located at the Aha Reservoir (AHR) on the Wujiang River in southwestern China (26°32′3.44″ N, 106°38′46.54″ E) and the Guanshan Lake (GSL) (26°38′20.57″ N, 106°37′55.18″ E) (Figure 1), situated within the world's largest karst region [33]. Both are located in the subtropical monsoon climate zone, with an average annual rainfall of 1140 mm to 1200 mm and an average temperature of 23.2 °C [34]. AHR is an open-type artificial reservoir situated on the Xiaohe River, a tributary of the Nanming River in southern Guiyang City, belonging to the Wujiang River Basin [35]. In this study, an open reservoir is defined as a water body with both surface inflow and outflow rivers, resulting in strong hydrological connectivity with its watershed. AHR receives water from multiple tributaries and discharges downstream through surface channels, thus representing a typical open reservoir. This karst basin is characterized by Triassic dolomite, limestone, and carbonate formations [36]. Its five main tributaries are the Jinzhong River (R1), Youyu River (R2), Baiyan River (R3), Caichong River (R4), and Lanni River (R5) [25]. Among these, R1 experiences significant anthropogenic disturbances primarily from urban industrial and domestic wastewater, whereas R2 and R3 are mainly influenced by coal mine effluent discharges [34]. With a catchment area of 190 km^2 and a storage capacity of 54 million m^3, AHR has an average depth of approximately 13 m [37] and mainly functions in urban water supply and flood control. The region receives abundant rainfall, with frequent summer storms and persistent winter drizzle.

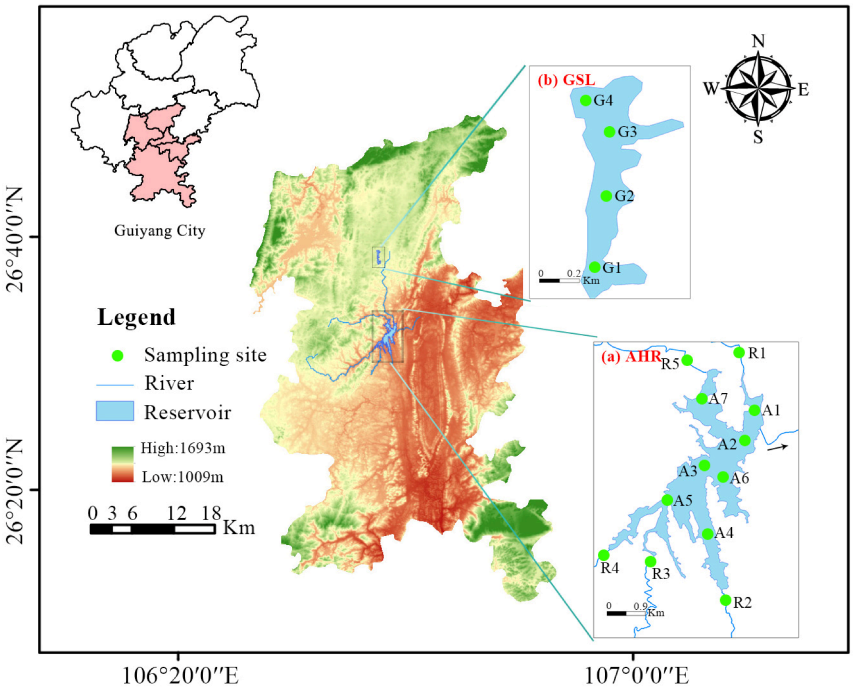


Figure 1. Study area and sampling locations. (**a**) Distribution of sampling sites in AHR (including the five major inflow rivers: R1 Jinzhong River, R2 Lanni River, R3 Caichong River, R4 Youyu River, and R5 Baiyan River; the arrow indicates the flow direction of the outflow river, the Xiaoche River). (**b**) Distribution of sampling sites in GSL.

GSL is a closed, artificial scenic lake (also known as Guanshan Reservoir), located in the central area of Guanshanhu District, Guiyang City. In this study, a closed reservoir is defined as a water body lacking permanent surface inflow and outflow rivers and being supplied primarily by groundwater seepage/springs and precipitation. GSL has no major surface inflow or outflow channels and is mainly fed by underground mountain springs [38], representing a typical closed reservoir with relatively weak hydrological connectivity. It covers a water surface area of approximately 0.2 km^2 and has an average water depth of 1–2 m. The lake is surrounded by lush forests with abundant forest resources. The wetland area of Guanshanhu Wetland Park, where the lake is located, covers approximately 40 ha.

2.2. Sample Collection and Bulk Geochemical Analyses

2.2.1. Sample Collection

Surface water samples were collected from a depth of 0.5 m at all sampling locations, including the seven sites (A1–A7) evenly distributed in AHR (with A2 located in the dam convergence zone), the five major inflowing rivers of the reservoir, and the four sites (G1–G4) in GSL (Figure 1). Sampling buckets were rinsed three times with reservoir water before collecting 4-L water samples at each sampling site, ensuring that the bottles were completely filled without air bubbles. Sealed bags (polyethylene zip-top bags; Hefei Mingyang Plastic Co., Ltd., Hefei, China) were used to collect surface soil and surrounding plant samples. In addition, the Hydrolab multi-parameter water-quality analyzer (Hydrolab HL7; OTT Hydromet, Loveland, CO, USA) was used to measure the pH, temperature (T), dissolved oxygen (DO), conductivity (EC), turbidity (Turb.), and chlorophyll a (Chl.a) of the water body on site.

2.2.2. Analytical Methods

Water samples were filtered through pre-combusted 0.45 μm cellulose acetate membrane filters (Whatman, Maidstone, UK). For DIC analysis, a 300 mL filtered water sample was transferred into a vacuum-sealed conical flask and evacuated to $<10^{-2}$ torr. Subsequently, 20–25 mL of 85% phosphoric acid (Sinopharm Chemical Reagent Co., Ltd., Shanghai, China) was injected, and the liberated CO_2 was quantitatively extracted under vacuum. No carrier gas (e.g., N_2 or He) was used during this process. The generated CO_2 was purified using a vacuum line, including water removal with an isopropanol-liquid nitrogen cold trap and sulfur removal by heated copper when necessary [39]. The purified CO_2 was collected in a calibrated volume and divided into two aliquots for $\delta^{13}C$ and $\Delta^{14}C$ analyses [40]. DIC concentration was calculated using the ideal gas law ($pV = nRT$). For AHR, DIC concentration and isotopic data were obtained from our previously published study [25].

For DOC analysis, 2 L of filtered water was transferred into a vacuum reaction system. To remove DIC, 5 mL of 85% phosphoric acid was added under vacuum conditions ($<1 \times 10^{-2}$ bar), and the released CO_2 was completely removed by vacuum degassing. The remaining sample was concentrated to approximately 20 mL at 50 °C. Subsequently, 5 mL of sodium persulfate oxidant (99.99%; Aladdin Industrial Corporation, Shanghai, China) was added, and the sample was heated at 95 °C for 30 min to oxidize DOC into CO_2. The generated CO_2 was purified using the same vacuum-line procedure described above. The total carbon mass was calculated from the measured pressure and volume using the ideal gas law, and the entire recovered CO_2 was divided into two aliquots for $\delta^{13}C$ and $\Delta^{14}C$ measurements. Surface soil samples were oven-dried at 60 °C to constant weight (24 h) and ground in an oven (DHG-9140A; Shanghai Jinghong Laboratory Equipment Co., Ltd., Shanghai, China). Approximately 10 g of each dried soil sample was treated with hydrochloric acid (37%; Sinopharm Chemical Reagent Co., Ltd., Shanghai, China) for 24 h

to remove inorganic carbon. After repeated rinsing with ultrapure water to neutrality, the samples were dried, reground, combusted in a vacuum system, and purified to obtain CO_2 for isotope analysis. Plant samples were cleaned, oven-dried at 60 °C to constant weight, ground, treated with 1 mol/L HCl for 12 h, rinsed to neutrality, and combusted using the same vacuum procedure. The resulting CO_2 from both soil and plant samples was divided into two aliquots for $\delta^{13}C$ and $\Delta^{14}C$ determinations.

The $\delta^{13}C$ value of algal organic carbon was assigned an empirical value of $-30 \pm 1‰$ [31], whereas its $\Delta^{14}C$ value was represented by the $\Delta^{14}C$ value of DIC in the corresponding water body [23,41]. $\delta^{13}C$ values were measured using a MAT251 stable isotope ratio mass spectrometer (Finnigan MAT, Bremen, Germany) at the Institute of Earth Environment, Chinese Academy of Sciences. For $\Delta^{14}C$ analysis, purified CO_2 was reduced to graphite using zinc (analytical grade; Sinopharm Chemical Reagent Co., Ltd., Shanghai, China) as reductant and iron powder (analytical grade; Sinopharm Chemical Reagent Co., Ltd., Shanghai, China) as catalyst. The graphite targets were measured using a 3 MV accelerator mass spectrometer (AMS) (model 3MV Tandetron, High Voltage Engineering Europa B.V., Amsterdam, The Netherlands) at the Xi'an AMS center. To evaluate potential atmospheric carbon contamination during sample preparation, procedural blanks were assessed following [42]. Anthracite, wood, and lacustrine sediment samples with expected radiocarbon ages older than 50,000 yr BP were subjected to the same pretreatment and combustion procedures. The resulting blank values corresponded to $F^{14}C \approx 0.002$ (<0.2% modern carbon contamination), indicating negligible effects on the measured $\Delta^{14}C$ values.

Field sampling points were geolocated using handheld GPS devices, with distribution maps generated through ArcGIS 10.8 and QGIS 3.16. Data analysis and visualization were performed employing the R 4.4.3, Origin 2021, and IBM SPSS Statistics 25. Significant differences between groups (e.g., AHR vs. GSL) were assessed using independent *t*-tests and one-way ANOVA, with significance levels set at $p < 0.05$ and $p < 0.01$. All statistical comparisons were pre-planned pairwise comparisons (e.g., AHR vs. GSL). Original *p*-values are reported with significance levels ($p < 0.05$ and $p < 0.01$). The contribution rates of DOC source end-members were calculated using the IsoSource end-member mixing model.

3. Results

3.1. The Basic Physical and Chemical Parameters

The mean values of T, pH, Chl.a, Turb., EC and DO in AHR were 9.44 ± 0.19 °C, 7.60 ± 0.23, 13.10 ± 3.29 μg/L, 8.96 ± 2.37 NTU, 552.26 ± 8.07 μS/cm and 9.85 ± 0.55 mg/L, respectively (Figure 2). The inflow rivers of AHR exhibited mean values of T, pH, Chl.a, Turb., EC and DO of 10.60 ± 0.55 °C, 7.55 ± 0.57, 5.19 ± 2.14 μg/L, 9.22 ± 2.97 NTU, 637.70 ± 170.17 μS/cm, and 10.72 ± 1.34 mg/L, respectively (Figure 2). In GSL, the mean values of T, pH, Chl.a, Turb., EC and DO were 2.82 ± 2.27 °C, 7.47 ± 0.15, 103.00 ± 29.87 μg/L, 13.23 ± 2.28 NTU, 422.85 ± 15.54 μS/cm, and 11.34 ± 0.31 mg/L, respectively (Figure 2). Detailed physical and chemical parameters for each water body are presented in Table A1. Comparative analysis revealed that GSL had lower T and EC but higher pH, Chl.a, Turb. and DO values than AHR. AHR is an open reservoir, while GSL is relatively closed. The higher EC in AHR likely results from river inflows that carry a large quantity of ions from the watershed. For instance, the R4 watershed, characterized by elevated EC values, contains several abandoned coal mines and coal-bearing strata. Although mining activities ceased decades ago, acid mine drainage continues to discharge from these areas, contributing to the high ionic load. Chl.a is an important indicator of primary productivity in aquatic systems and reflects algal biomass [43]. The high Chl.a content in GSL influenced its water transparency, resulting in high Turb. values. This

indicates strong photosynthetic activity in GSL, promoting the conversion of inorganic carbon into organic carbon.

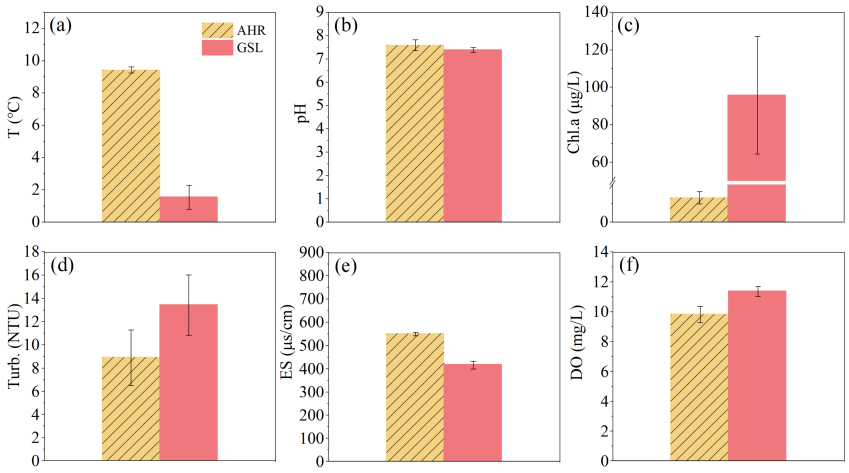


Figure 2. The basic physical and chemical parameters. (**a**) T; (**b**) pH; (**c**) Chl.a; (**d**) Turb.; (**e**) ES; (**f**) DO.

3.2. The Content of DOC and DIC

The DOC concentration in the inflowing rivers ranged from 0.15 mg/L to 2.36 mg/L, with an average of 1.47 ± 0.72 mg/L (Table A1). The DOC content in AHR ranged from 2.84 mg/L to 3.83 mg/L, with an average of 3.37 ± 0.30 mg/L (Figure 3a). The DOC content at different sampling sites was as follows: A3 (3.83 mg/L) > A6 (3.55 mg/L) > A4 (3.52 mg/L) > A7 (3.45 mg/L) > A1 (3.36 mg/L) > A5 (3.07 mg/L) > A2 (2.84 mg/L) (Table A1). The DOC content in GSL ranged from 3.75 mg/L to 4.54 mg/L, with an average of 4.14 ± 0.28 mg/L (Figure 3a). From highest to lowest, the site sequence was G2 (4.54 mg/L) > G1 (4.20 mg/L) > G4 (4.08 mg/L) > G3 (3.75 mg/L) (Table A1). Compared with AHR, GSL exhibited significantly higher DOC concentrations (Figure 3a; $p < 0.01$). The DIC concentration in GSL varied from 14.19 mg/L to 27.44 mg/L, with an average of 23.78 ± 5.56 mg/L, showing no significant difference from that in AHR (Figure 3b; $p > 0.05$).

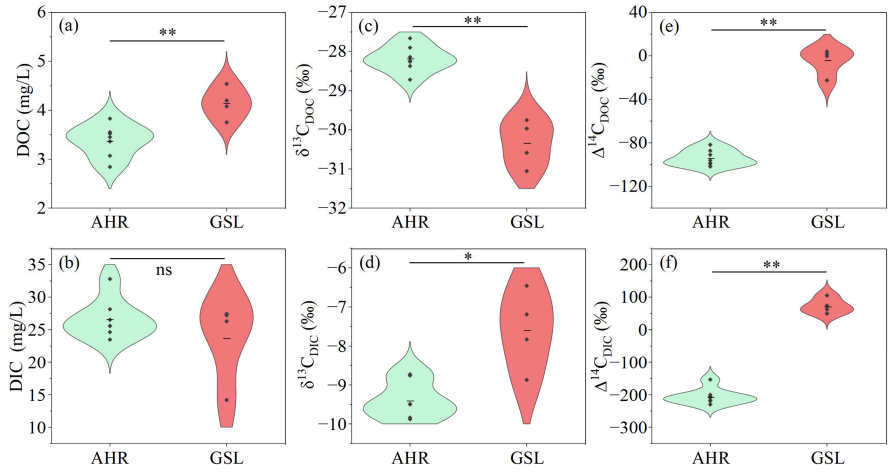


Figure 3. Concentrations and $\delta^{13}C$–$\Delta^{14}C$ values of DOC and DIC. (**a**) DOC concentration; (**b**) DIC concentrations (**c**) $\delta^{13}C_{DOC}$; (**d**) $\delta^{13}C_{DIC}$; (**e**) $\Delta^{14}C_{DOC}$; (**f**) $\Delta^{14}C_{DIC}$. "ns" denotes no significant difference; single asterisk (*) indicates a significant difference ($p < 0.05$), and double asterisks (**) indicate a highly significant difference ($p < 0.01$).

3.3. The $\delta^{13}C$ Composition

The $\delta^{13}C$ values of DOC in AHR ranged from −28.72‰ to −27.66‰, with an average of −28.18 ± 0.31‰ (Figure 3c). Across sampling sites, $\delta^{13}C$ values decreased in the following order: A1 (−27.66‰) > A2 (−27.90‰) > A3 (−28.14‰) > A5 (−28.24‰) > A7 (−28.26‰) > A6 (−28.37‰) > A4 (−28.72‰) (Table A1). The $\delta^{13}C$ values of DOC in the inflow rivers ranged from −30.80‰ to −26.86‰, with an average of −28.46 ± 1.40‰ (Table A1). Although R1 is closer to A1 and A2, there was a distinct difference in their $\delta^{13}C$ values. The relatively positive $\delta^{13}C$ values at A1 and A2 may be caused by the dissolution of calcium carbonate transported by rivers, which increases the $\delta^{13}C$ values of DIC and consequently those of DOC. The $\delta^{13}C$ values of DOC in AHR overlapped most closely with those of plants (−27.98 ± 0.13‰), were more negative than those of soil (−26.51 ± 1.57‰), and more positive than those of algae (−30 ± 1‰) (Figure 4). Moreover, the similar $\delta^{13}C$ values among AHR, its inflow rivers, and plants suggest that plant-derived organic matter is transported into the reservoir via riverine input.

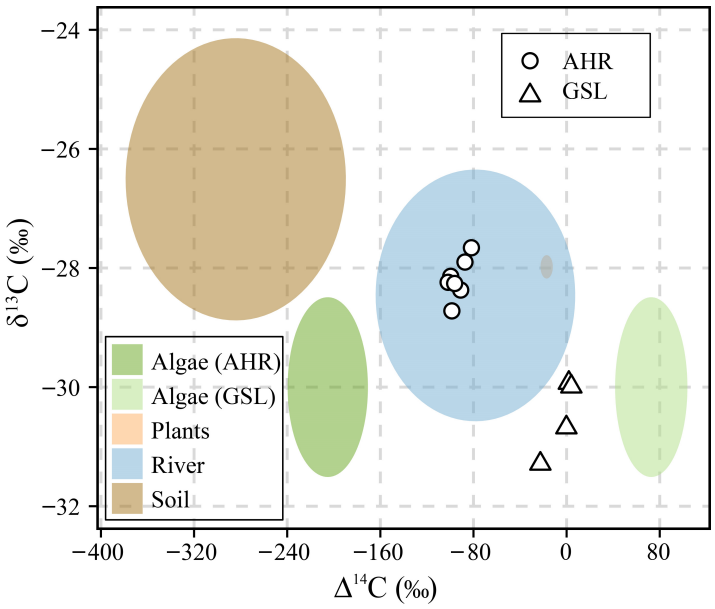


Figure 4. Cross-plot of $\delta^{13}C$–$\Delta^{14}C$ values for DOC source end-members.

In GSL, the $\delta^{13}C$ values of DOC ranged from −31.29‰ to −29.93‰, with a mean of −30.34 ± 0.51‰ (Figure 3c), clustering near algal-derived values (−30.13 ± 0.70‰). Spatially, $\delta^{13}C$ values decreased in the following order: G3 (−29.93‰) > G4 (−29.96‰) > G2 (−30.68‰) > G1 (−31.29‰) (Table A1), showing a decreasing trend from the northern to the southern part of the lake. DOC in GSL exhibited significantly lower $\delta^{13}C$ values than DOC in AHR (Figure 3c; $p < 0.01$). Additionally, the $\delta^{13}C$ values of DIC in GSL (−8.87‰ to −6.46‰, mean −7.59 ± 0.88‰) were significantly more enriched than those in AHR (−9.88‰ to −8.73‰, mean −9.38 ± 0.43‰) (Figure 3d; $p < 0.05$), clarifying the differences in DOC sources and carbon cycling processes between the two systems.

3.4. The $\Delta^{14}C$ Composition

The $\Delta^{14}C$ values of DOC in AHR ranged from −101.79‰ to −81.78‰, with an average of −93.74‰ ± 6.76‰ (Figure 3f). Across sampling sites, $\Delta^{14}C$ values decreased in the following order: A1 (−81.78‰) > A2 (−87.32‰) > A6 (−90.99‰) > A7 (−96.18‰) > A4 (−98.56‰) > A3 (−99.55‰) > A5 (−101.79‰) (Table A1). The $\Delta^{14}C$ values of DOC in inflow rivers ranged from −97.06‰ to 18.57‰, with an average of −78.33 ± 56.78‰ (Table A1). Among these, the $\Delta^{14}C$ value of DOC from R1 indicated a modern carbon

signal, while the others were negative, with R4 showing the most negative value. Since A1 and A2 are close to R1, their positive $\Delta^{14}C$ values were likely influenced by R1. Similarly, the relatively negative $\Delta^{14}C$ value of A5 may also be attributed to the influence of R4. The $\Delta^{14}C$ values of DOC in AHR were most similar to those of plants (-17.14 ± 3.49‰), followed by algae (-205.16 ± 22.85‰), and showed the greatest discrepancy with soil (-284.20 ± 62.67‰) (Figure 4). The $\Delta^{14}C$ values of DOC in the inflow rivers of AHR show significant overlap with those of plants and DOC, following the same pattern as the $\delta^{13}C$ values. This further suggests that plant organic carbon is transported into the reservoir via the rivers.

The $\Delta^{14}C$ values of DOC in GSL were significantly more positive than those in AHR (Figure 3e; $p < 0.01$), ranging from -22.55‰ to 4.07‰, with an average of -6.94 ± 11.07‰ (Figure 3f). Within GSL, the $\Delta^{14}C$ values of DOC show a trend of becoming higher from the northern to the southern regions. The $\Delta^{14}C$ values of DOC in GSL exhibit significant overlap with those of algae (Figure 4), suggesting that this phenomenon may be attributed to algal photosynthesis. The $\Delta^{14}C$ values of DIC in GSL range from 49.54‰ to 105.12‰, with an average of 72.71 ± 20.57‰, which is extremely significantly positive compared to the $\Delta^{14}C$ values of DIC in AHR (ranging from -230.25‰ to -153.83‰, with an average of -205.16 ± 22.85‰) (Figure 3f; $p < 0.01$).

4. Discussion

4.1. Significant Differences in DOC Sources Between Open and Closed Reservoirs

Based on the IsoSource mixing model calculation, the primary source of DOC in AHR was plants (61 ± 2%; Figure 5a; $p < 0.05$), followed by algae (27 ± 4%) and soil (12 ± 4%) (Figure 5a). These source proportions were calculated using the isotopic end-member values shown in Figure 4. Previous studies indicate that modern vegetation is the dominant source of riverine DOC, contributing as much as 99% in the Heilongjiang River [44,45]. The similar DOC isotopic signatures between AHR and its inflowing rivers further support this finding. The carbon transported by river erosion from watershed vegetation is enriched in aromatic compounds and other substances that are resistant to microbial degradation but susceptible to photodegradation [13]. Spatial variations in DOC source contributions were also observed. For instance, at site A2 near the dam where waters are quiescent, algal contributions were elevated (28%) while soil inputs were relatively low (7%), likely associated with localized algal activity. In contrast, plant-derived DOC contributions exhibited minimal spatial variation across all sites, ranging from 60% to 67% (Figure A1).

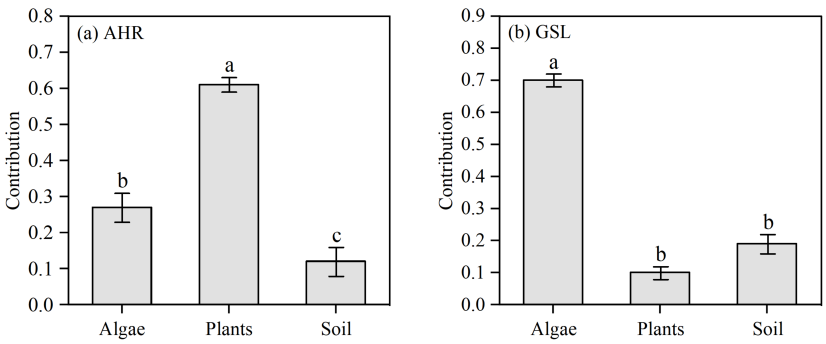


Figure 5. Proportional contributions of different DOC sources. (**a**) Proportional contributions of DOC sources in GSL; (**b**) Proportional contributions of DOC sources in AHR. Different letters above the bars indicate significant differences ($p < 0.05$).

In contrast to AHR, algae represented the dominant source of DOC in GSL (70 ± 2%; Figure 5b; $p < 0.05$). Soil (19 ± 3%) and plants (10 ± 2%) were minor contributing sources,

with no significant difference between their contribution rates ($p > 0.05$), and the proportions of DOC sources remained relatively consistent across different sampling sites. GSL is less influenced by watershed erosion, receiving limited inputs from terrestrial plants and soils. Consequently, its DOC primarily originates from in situ algal production. The lake exhibits high primary productivity (Chl. a = 103.00 ± 29.87 μg/L) and weak water circulation, both of which reflect strong algal activity and consequently promote DOC production [43,46]. This internally driven carbon dynamic is further supported by the consistent isotopic patterns of both DIC and DOC in GSL, which show more negative $\delta^{13}C$ values and more positive $\Delta^{14}C$ values compared with those in AHR. The more negative $\delta^{13}C$ values arise from the preferential assimilation of ^{12}C during algal photosynthesis, which produces DOC with lighter isotopic signatures [47]. At the same time, the intensified photosynthetic activity in GSL enhances ^{13}C fractionation between DOC and DIC, producing more negative $\delta^{13}C$ values in DOC and a greater isotopic offset between DOC and DIC than in AHR. Furthermore, intense photosynthesis in GSL likely lowers the partial pressure of dissolved CO_2, thereby facilitating the absorption of modern atmospheric CO_2 (with positive $\Delta^{14}C$) and leading to the positive $\Delta^{14}C$ values observed in both DIC and its derivative DOC [48].

4.2. Enhanced BCP Effect Reduces CO_2 Emission Potential in GSL

Differences may exist in the sources of inorganic carbon converted to DOC via the BCP in GSL and AHR. Phytoplankton typically preferentially utilize aqueous CO_2 as their carbon source, but may resort to HCO_3^- under high carbon demand conditions [47,48]. The organic carbon produced by algae using CO_2 has a negative $\delta^{13}C$ value [47], which also causes the $\delta^{13}C$ value of the remaining HCO_3^- to be positive. Therefore, DOC produced by algae using HCO_3^- as a carbon source has a positive $\delta^{13}C$ value [49]. In AHR, the $\delta^{13}C$ value of DOC was negatively correlated with Chl.a content (Figure 6a; $R^2 = 0.49$), indicating that the algae in this reservoir primarily rely on CO_2. In contrast, the $\delta^{13}C$ value of DOC in GSL showed a positive correlation with Chl.a content (Figure 6a; $R^2 = 0.97$), indicating that algae in GSL not only utilize CO_2 but also HCO_3^-. Additionally, the $\Delta^{14}C$ values of DOC in GSL are positively correlated with Chl.a content, while the $\Delta^{14}C$ values of DIC are also positively shifted, suggesting that CO_2 with a positive $\Delta^{14}C$ bias from the atmosphere enters the water and is assimilated into organic carbon [26,48]. This is likely due to the high primary productivity in GSL, where algae consume large amounts of CO_2, reducing the CO_2 partial pressure in the water below atmospheric levels [50,51], thereby facilitating the diffusion of atmospheric CO_2 into the water. The $\Delta^{14}C$ values of DOC in AHR showed a weak negative correlation with Chl.a content (Figure 6b; $R^2 = 0.12$), indicating that the water has relatively abundant CO_2 and has not significantly absorbed atmospheric CO_2. Overall, the carbon sources supporting algal production differ markedly between the two reservoirs. Algae in GSL utilize both dissolved CO_2 and HCO_3^-, thereby promoting the influx of atmospheric CO_2. In contrast, algae in AHR primarily rely on dissolved CO_2. This indicates that GSL has a greater carbon sequestration capacity.

In addition, the decomposition processes of DOC may differ between the two reservoirs. DOC can decompose via photochemical and microbial pathways, and the resulting CO_2 is partitioned between conversion to DIC and evasion to the atmosphere [51]. At AHR, DIC and DOC content showed a weak positive correlation (Figure 6c; $R^2 = 0.08$), while their $\delta^{13}C$ values showed a strong positive correlation (Figure 6d; $R^2 = 0.76$), suggesting that a portion of the DIC was derived from DOC decomposition. Due to lower algal CO_2 demand in AHR, DOC decomposition is likely to elevate the partial pressure of aqueous CO_2. In contrast, GSL exhibited inverse relationships between DIC and DOC in both concentration and $\delta^{13}C$ values (Figure 6c,d). This pattern can be attributed to the strong BCP effect in GSL, which results in high CO_2 demand. As a result, CO_2 produced by DOC decomposition

is rapidly assimilated by algae, reducing its conversion to DIC and resulting in low DIC content (23.78 ± 5.56 mg/L) [37]. This process also reduces CO_2 release from GSL into the atmosphere, consistent with the findings of Shao et al. [27]. Therefore, although DOC decomposition occurs in both reservoirs, AHR may pose a carbon emission risk, while GSL effectively recycles the carbon produced by DOC decomposition through a strong BCP effect, thereby reducing carbon emissions.

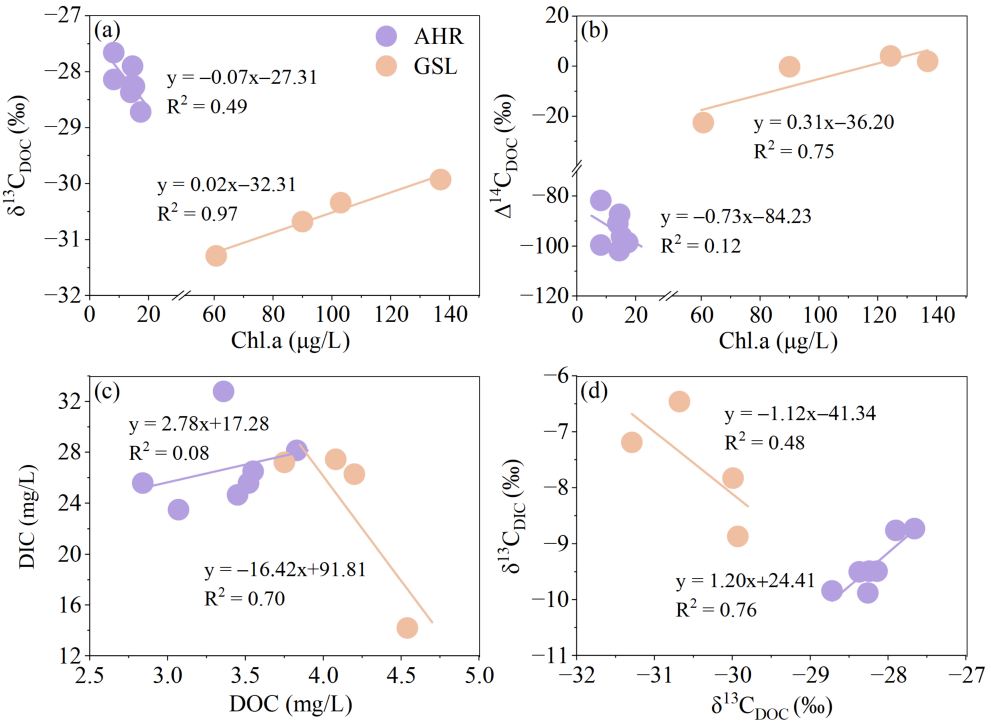


Figure 6. Correlation analysis among $\delta^{13}C$, $\Delta^{14}C$, Chl.a, DOC and DIC. (**a**) Correlation between $\delta^{13}C_{DOC}$ and Chl.a; (**b**) Correlation between $\Delta^{14}C_{DOC}$ and Chl.a; (**c**) Correlation between DIC and DOC; (**d**) Correlation between $\delta^{13}C_{DIC}$ and $\delta^{13}C_{DOC}$.

4.3. WRT as a Driver of Elevated DOC in GSL

The DOC concentration in GSL was significantly higher than that in AHR (4.14 ± 0.28 mg/L > 3.37 ± 0.30 mg/L). This discrepancy may be attributed to the higher proportion of recalcitrant DOC (RDOC) in GSL. RDOC consists of byproducts and derivatives (e.g., carboxyl-rich alicyclic molecules) generated during microbial degradation of DOC, exhibiting high stability with turnover times of up to thousands of years [52]. Moreover, autochthonous DOC in reservoirs is more readily utilized by microorganisms compared to allochthonous DOC [53], undergoing continuous transformation into RDOC. Studies demonstrate that recalcitrant dissolved organic matter derived from the transformation of autochthonous dissolved organic matter can account for up to 89.6% [8]. Therefore, GSL, with a substantially higher proportion of autochthonous DOC (70 ± 2%) than AHR (27 ± 4%), is likely more favorable for RDOC formation. These findings suggest that DOC in GSL is more stable than that in AHR, favoring its long-term preservation in the water body and consequently higher DOC concentrations.

Differences in WRT likely represent the key factor controlling DOC concentration and composition between the two reservoirs. AHR exhibits superior hydrological connectivity, whereas GSL demonstrates a stronger BCP effect, with more positive $\Delta^{14}C$ values in DIC (72.71 ± 20.57‰). These characteristics all support the idea that GSL has a longer WRT [27,54]. Previous studies estimated the WRT of AHR to be approximately 201 days [55]. Although no direct estimate is available for GSL, its WRT can be approximated using the

closed-reservoir model proposed by Liu et al. [54], where WRT is calculated as mean depth divided by annual evaporation. Using a mean depth of 1.5 m for GSL and an annual evaporation rate of 843.4 mm in Guiyang [56], the estimated WRT is approximately 650 days. The shorter WRT and good connectivity in AHR result in higher DOC flux, making it difficult for RDOC to remain in the water. As a result, DOC is predominantly composed of active components [57]. These active components decompose more readily, with ^{12}C being preferentially utilized by microorganisms during decomposition [58], which leads to a negative $\delta^{13}C$ value of DIC in AHR ($-9.38 \pm 0.43‰$). Moreover, the longer WRT in GSL promotes the production of more autochthonous DOC, which in turn facilitates the generation of more RDOC. RDOC, which is less susceptible to loss from the water column, can accumulate more readily [57]. Furthermore, evaporation may further concentrate DOC in the reservoir, thereby increasing its content in the reservoir. Other studies have identified similar patterns. For example, Shao et al. [27] found that the DOC content in the Wuli River Reservoir, which has a longer WRT, was higher than that in the Honghe Reservoir.

Notably, AHR is situated in an urban center and subject to greater anthropogenic influence than GSL; if anthropogenic nutrient inputs were the dominant control on reservoir productivity, AHR would be expected to exhibit higher primary productivity [59]. However, the higher Chl. a concentration observed in GSL (Figure 2c) argues against this interpretation and instead reinforces the role of WRT as the primary driver, given that longer WRT favors sustained algal activity. We therefore consider it unlikely that anthropogenic inputs confound the fundamental open-versus-closed comparison, although future studies incorporating detailed watershed land-use data would help further constrain these contributions. In conclusion, the longer WRT in GSL is a key factor contributing to higher DOC concentrations, with the primary mechanisms involving the formation of RDOC and the enrichment of DOC due to water evaporation.

5. Conclusions

By employing a dual carbon isotope approach, this study demonstrates that hydrological connectivity fundamentally dictates DOC cycling patterns in karst reservoirs. While the open AHR relies predominantly on allochthonous riverine inputs, the prolonged WRT in the closed GSL fosters a system dominated by autochthonous algal production. Crucially, this extended WRT stimulates a more vigorous BCP effect. This not only accelerates the conversion of inorganic carbon to organic carbon—thereby mitigating CO_2 emission potential—but also drives the continuous formation and accumulation of RDOC. Consequently, these coupled processes yield higher DOC concentrations and enhanced stability, establishing closed karst reservoirs as significantly more robust carbon sinks than their open counterparts.

However, to overcome the constraints of localized sample sizes and indirect mechanistic inferences, future research should apply this comparative framework across a wider array of karst reservoirs. Integrating stable hydrogen and oxygen isotopes (δ^2H and $\delta^{18}O$) for quantitative WRT constraints, alongside ultra-high-resolution analytical techniques (e.g., FT-ICR MS or EEMs-PARAFAC) for DOC molecular characterization, will be imperative. Such multidisciplinary efforts are essential for the precise quantification of inland-water carbon sinks and will deliver robust empirical data to refine and evaluate regional karst carbon sink models.

Author Contributions: Conceptualization, X.Y.; methodology, X.Y. and H.L.; software, B.D. and X.L.; validation, H.L., M.S. and Y.A.; formal analysis, X.Y. and H.L.; investigation, B.D., X.L., Z.M., C.M. and C.Y.; resources, M.S. and Y.A.; data curation, X.Y.; writing—original draft preparation, X.Y. and H.L.; writing—review and editing, X.Y. and H.L.; visualization, H.L., B.D., X.L., Z.M., C.M.

and C.Y.; funding acquisition, X.Y. All authors have read and agreed to the published version of the manuscript.

Funding: This research was funded by the Guizhou Provincial Science and Technology Support Program, grant number QianKeHeJiChu-ZK [2024] YiBan511, and the Research Initiation Program for High-level Talents of Guizhou Institute of Technology in 2023, grant number 2023GCC082.

Data Availability Statement: Data will be made available on request.

Acknowledgments: We thank reviewers and the Editor-in-Chief for their constructive comments.

Conflicts of Interest: The authors declare no conflicts of interest.

Abbreviations

The following abbreviations are used in this manuscript:

AHR	Aha Reservoir
AMS	Accelerator mass spectrometry
AOC	Autochthonous organic carbon
BCP	Biological carbon pump
Chl.a	Chlorophyll a
$\Delta^{14}C$	Radiocarbon isotopic composition (Radiocarbon)
$\delta^{13}C$	Stable carbon isotopic composition
DIC	Dissolved inorganic carbon
DO	Dissolved oxygen
DOC	Dissolved organic carbon
EC	Conductivity (Electrical Conductivity)
GSL	Guanshan Lake
POC	Particulate organic carbon
RDOC	Recalcitrant dissolved organic carbon
T	Temperature
Turb.	Turbidity
WRT	Water retention time

Appendix A

Table A1. Comprehensive characterization of water physicochemical parameters, carbon content, and $\delta^{13}C$–$\Delta^{14}C$ values. R1–R5: Inflow rivers; A1–A7: Aha Reservoir sites; G1–G4: Guanshan Lake sites.

Sampling Sites	T (°C)	pH	Chl.a (μg L^{-1})	Turb. (NTU)	EC (μs cm^{-1})	DO (mg L^{-1})	DOC (mg L^{-1})	$\delta^{13}C_{DOC}$ (‰)	$\Delta^{14}C_{DOC}$ (‰)	DIC (mg L^{-1})	$\delta^{13}C_{DIC}$ (‰)	$\Delta^{14}C_{DIC}$ (‰)
R1	11.36	8.13	6.43	7.1	648.6	9.85	2.36	−29.20	18.57	44.42	−10.33	9.77
R2	10.27	6.50	2.07	15.0	640.6	9.62	1.56	−27.50	−94.75	48.60	−11.66	−265.53
R3	10.64	7.56	6.94	7.3	568.8	13.32	1.58	−30.80	−97.06	24.42	−9.87	−223.65
R4	10.98	7.58	3.20	9.1	928.3	10.17	0.15	−26.86	−155.05	28.60	−8.12	−458.44
R5	9.77	8.00	7.32	7.6	402.2	10.66	1.72	−27.96	−63.36	22.79	−9.85	−154.89
A1	9.81	7.08	8.14	4.4	550.5	8.86	3.36	−27.66	−81.78	32.79	−8.73	−153.83
A2	9.39	7.61	14.57	7.5	551.5	9.34	2.84	−27.90	−87.32	25.58	−8.76	−200.45
A3	9.50	7.50	8.15	8.9	553.5	10.32	3.83	−28.14	−99.55	28.14	−9.49	−216.85
A4	9.24	7.74	17.30	9.7	549.3	10.31	3.52	−28.72	−98.56	25.58	−9.84	−208.78
A5	9.46	7.63	14.44	9.0	570.7	9.76	3.07	−28.24	−101.79	23.49	−9.49	−230.25
A6	9.51	7.80	13.93	12.6	545.5	9.82	3.55	−28.37	−90.99	26.51	−9.50	−206.10
A7	9.17	7.81	15.20	10.6	544.8	10.52	3.45	−28.26	−96.18	24.65	−9.88	−219.88
G1	1.19	7.26	60.67	9.8	396.3	10.95	4.20	−31.06	−22.55	26.28	−7.19	49.54
G2	0.90	7.40	90.03	15.3	434.5	11.49	4.54	−30.59	−0.20	14.19	−6.46	73.70
G3	2.59	7.54	136.94	15.3	427.6	11.76	3.75	−29.75	1.91	27.21	−8.87	62.47
G4	6.60	7.66	124.35	12.5	433.0	11.15	4.08	−29.97	4.07	27.44	−7.83	105.12

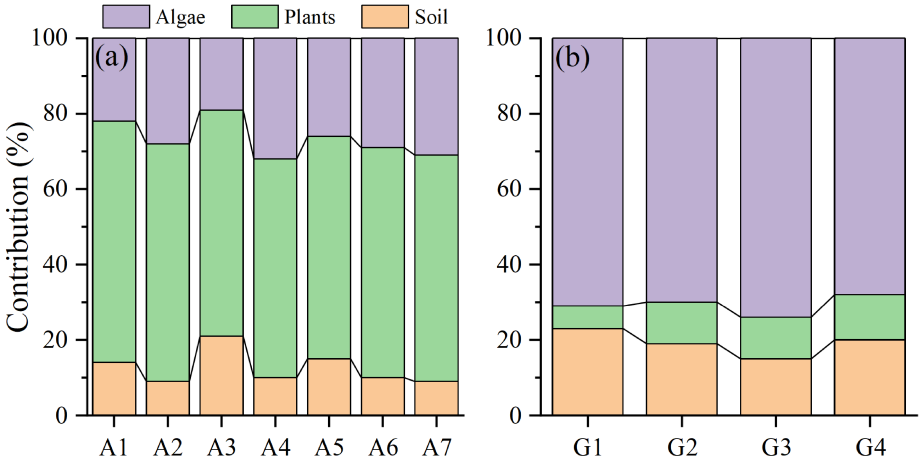


Figure A1. Site-specific proportional contributions of different DOC sources for (**a**) Aha Reservoir (AHR) and (**b**) Guanshan Lake (GSL).

References

1. He, Q.; Xiao, Q.; Fan, J.; Zhao, H.; Cao, M.; Zhang, C.; Jiang, Y. The impact of heterotrophic bacteria on recalcitrant dissolved organic carbon formation in a typical karstic river. *Sci. Total Environ.* **2022**, *815*, 152576. [CrossRef] [PubMed]
2. Jiao, N.; Herndl, G.J.; Hansell, D.A.; Benner, R.; Kattner, G.; Wilhelm, S.W.; Kirchman, D.L.; Weinbauer, M.G.; Luo, T.; Chen, F.; et al. Microbial production of recalcitrant dissolved organic matter: Long-term carbon storage in the global ocean. *Nat. Rev. Microbiol.* **2010**, *8*, 593–599. [CrossRef] [PubMed]
3. Bade, D.L.; Carpenter, S.R.; Cole, J.J.; Pace, M.L.; Kritzberg, E.; Van de Bogert, M.C.; Cory, R.M.; McKnight, D.M. Sources and fates of dissolved organic carbon in lakes as determined by whole-lake carbon isotope additions. *Biogeochemistry* **2007**, *84*, 115–129. [CrossRef]
4. Leenheer, J.A.; Croué, J.-P. Characterizing aquatic dissolved organic matter. *Environ. Sci. Technol.* **2003**, *37*, 18A–26A. [CrossRef]
5. Nai, H.; Zhong, J.; Yi, Y.; Lai, M.; He, D.; Dittmar, T.; Liu, C.-Q.; Li, S.-L.; Xu, S. Anthropogenic disturbance stimulates the export of dissolved organic carbon to rivers on the Tibetan Plateau. *Environ. Sci. Technol.* **2023**, *57*, 9214–9223. [CrossRef] [PubMed]
6. Mendonça, R.; Müller, R.A.; Clow, D.; Verpoorter, C.; Raymond, P.; Tranvik, L.J.; Sobek, S. Organic carbon burial in global lakes and reservoirs. *Nat. Commun.* **2017**, *8*, 1694. [CrossRef] [PubMed]
7. Moody, C.S.; Worrall, F. Modeling rates of DOC degradation using DOM composition and hydroclimatic variables. *J. Geophys. Res. Biogeosci.* **2017**, *122*, 1175–1191. [CrossRef]
8. Xia, F.; Liu, Z.; Zhao, M.; He, H.; He, Q.; Lai, C.; He, X.; Ma, Z.; Wu, Y.; Ma, S. High stability of autochthonous organic matter in inland aquatic ecosystems. *J. Hydrol.* **2023**, *627*, 130407. [CrossRef]
9. Ni, M.; Li, S.; Santos, I.; Zhang, J.; Luo, J. Linking riverine partial pressure of carbon dioxide to dissolved organic matter optical properties in a Dry-hot Valley Region. *Sci. Total Environ.* **2020**, *704*, 135353. [CrossRef] [PubMed]
10. Raymond, P.A.; Bauer, J.E. Use of ^{14}C and ^{13}C natural abundances for evaluating riverine, estuarine, and coastal DOC and POC sources and cycling: A review and synthesis. *Org. Geochem.* **2001**, *32*, 469–485. [CrossRef]
11. Zigah, P.; McNichol, A.; Xu, L.; Johnson, C.; Santinelli, C.; Karl, D.; Repeta, D. Allochthonous sources and dynamic cycling of ocean dissolved organic carbon revealed by carbon isotopes. *Geophys. Res. Lett.* **2017**, *44*, 2407–2415. [CrossRef]
12. Hansen, A.M.; Kraus, T.E.C.; Pellerin, B.A.; Fleck, J.A.; Downing, B.D.; Bergamaschi, B.A. Optical properties of dissolved organic matter (DOM): Effects of biological and photolytic degradation. *Limnol. Oceanogr.* **2016**, *61*, 1015–1032. [CrossRef]
13. Stubbins, A.; Spencer, R.; Chen, H.; Hatcher, P.; Mopper, K.; Hernes, P.; Mwamba, V.; Mangangu, A.; Wabakanghanzi, J.; Six, J. Illuminated darkness: Molecular signatures of Congo River dissolved organic matter and its photochemical alteration as revealed by ultrahigh precision mass spectrometry. *Limnol. Oceanogr.* **2010**, *55*, 1467–1477. [CrossRef]
14. Wang, W.; Li, S.; Zhong, J.; Li, C.; Yi, Y.; Chen, S.; Ren, Y. Understanding transport and transformation of dissolved inorganic carbon (DIC) in the reservoir system using $\delta^{13}C_{DIC}$ and water chemistry. *J. Hydrol.* **2019**, *574*, 193–201. [CrossRef]
15. Liu, Z.; Dreybrodt, W.; Liu, H. Atmospheric CO_2 sink: Silicate weathering or carbonate weathering? *Appl. Geochem.* **2011**, *26*, S292–S294. [CrossRef]
16. Shih, Y.; Chen, P.; Lee, L.; Liao, C.; Jien, S.; Shiah, F.; Lee, T.; Hein, T.; Zehetner, F.; Chang, C.-T.; et al. Dynamic responses of DOC and DIC transport to different flow regimes in a subtropical small mountainous river. *Hydrol. Earth Syst. Sci.* **2018**, *22*, 6579–6590. [CrossRef] [PubMed]

17. Wang, W.; Li, S.-L.; Zhong, J.; Yi, Y.; Yue, F.; Han, Z.; Wu, Q.; He, D.; Liu, C.-Q. Unraveling the factors influencing CO_2 emissions from hydroelectric reservoirs in karst and non-karst regions: A comparative analysis. *Water Res.* **2024**, *248*, 120893. [CrossRef] [PubMed]
18. Chen, B.; Yang, R.; Liu, Z.; Sun, H.; Yan, H.; Zeng, Q.; Zeng, S.; Zeng, C.; Zhao, M. Coupled control of land uses and aquatic biological processes on the diurnal hydrochemical variations in the five ponds at the Shawan Karst Test Site, China: Implications for the carbonate weathering-related carbon sink. *Chem. Geol.* **2017**, *456*, 58–71. [CrossRef]
19. Maavara, T.; Akbarzadeh, Z.; Van Cappellen, P. Global dam-driven changes to riverine N: P: Si ratios delivered to the coastal ocean. *Geophys. Res. Lett.* **2020**, *47*, e2020GL088288. [CrossRef]
20. Xu, B.; Yang, D.; Yao, P.; Burnett, W.C.; Ran, X.; Charette, M.; Huang, X.; Liu, S.; Yu, Z. A new perspective for assessing water transport and associated retention effects in a large reservoir. *Geophys. Res. Lett.* **2018**, *45*, 9642–9650. [CrossRef]
21. Yang, M.; Liu, Z.; Sun, H.; Yang, R.; Chen, B. Organic carbon source tracing and DIC fertilization effect in the Pearl River: Insights from lipid biomarker and geochemical analysis. *Appl. Geochem.* **2016**, *73*, 132–141. [CrossRef]
22. Wu, Q.; Han, G. $\delta^{13}C_{DIC}$ tracing of dissolved inorganic carbon sources at Three Gorges Reservoir, China. *Water Sci. Technol.* **2018**, *77*, 555–564. [PubMed]
23. McCallister, S.L.; Bauer, J.E.; Cherrier, J.E.; Ducklow, H.W. Assessing sources and ages of organic matter supporting river and estuarine bacterial production: A multiple-isotope ($\Delta^{14}C$ and $\delta^{15}N$) approach. *Limnol. Oceanogr.* **2004**, *49*, 1687–1702. [CrossRef]
24. Chen, J.; Yang, H.; Zeng, Y.; Guo, J.; Song, Y.; Ding, W. Combined use of radiocarbon and stable carbon isotope to constrain the sources and cycling of particulate organic carbon in a large freshwater lake, China. *Sci. Total Environ.* **2018**, *625*, 27–38. [CrossRef] [PubMed]
25. Qiu, Z.; Wang, Q.; Liu, H.; Yu, X.; Wu, Q.; An, Y.; Cheng, P.; Zeng, J. Dual carbon isotopes ($\delta^{13}C$ and $\Delta^{14}C$) were used to reveal the main sources and input fluxes of dissolved inorganic carbon in a karst reservoir in winter. *Environ. Res.* **2024**, *262*, 119905. [CrossRef] [PubMed]
26. Liu, Z.; Zhao, M.; Sun, H.; Yang, R.; Chen, B.; Yang, M.; Zeng, Q.; Zeng, H. "Old" carbon entering the South China Sea from the carbonate-rich Pearl River Basin: Coupled action of carbonate weathering and aquatic photosynthesis. *Appl. Geochem.* **2017**, *78*, 96–104. [CrossRef]
27. Shao, M.; Liu, Z.; Sun, H.; Ma, Z.; Lai, C.; He, H.; Fang, Y.; Xia, F.; He, Q.; Liu, X.; et al. Multi-tracer evidence for the presence of autochthonous organic carbon and the role of biological carbon pump in two river–reservoir ecosystems on the Chinese Loess Plateau. *Chem. Geol.* **2023**, *635*, 121608. [CrossRef]
28. Liu, Z.; Macpherson, G.; Groves, C.; Martin, J.B.; Yuan, D.; Zeng, S. Large and active CO_2 uptake by coupled carbonate weathering. *Earth-Sci. Rev.* **2018**, *182*, 42–49. [CrossRef]
29. Li, W.; Wu, F.; Liu, C.; Fu, P.; Wang, J.; Mei, Y.; Wang, L.; Guo, J. Temporal and spatial distributions of dissolved organic carbon and nitrogen in two small lakes on the Southwestern China Plateau. *Limnology* **2008**, *9*, 163–171. [CrossRef]
30. Xu, D.; Chen, J.; Yang, H.; Wang, J.; Ji, Y. Stable Isotopic Composition and Distribution Characteristics of Organic Carbon in the Stratified Column of Lake Baihua, Guizhou Province. *Earth Environ.* **2014**, *42*, 597–603.
31. Zigah, P.; Minor, E.; Werne, J. Radiocarbon and stable-isotope geochemistry of organic and inorganic carbon in Lake Superior. *Glob. Biogeochem. Cycles* **2012**, *26*, GB1023. [CrossRef]
32. He, D.; Li, P.; He, C.; Wang, Y.; Shi, Q. Eutrophication and watershed characteristics shape changes in dissolved organic matter chemistry along two river-estuarine transects. *Water Res.* **2022**, *214*, 118196. [CrossRef] [PubMed]
33. Sun, J.; Takahashi, Y.; Strosnider, W.; Kogure, T.; Wu, P.; Cao, X. Tracing and quantifying contributions of end members to karst water at a coalfield in southwest China. *Chemosphere* **2019**, *234*, 777–788. [CrossRef] [PubMed]
34. Gao, S.; Wang, Z.; Wu, Q.; Zeng, J. Multivariate statistical evaluation of dissolved heavy metals and a water quality assessment in the Lake Aha watershed, Southwest China. *PeerJ* **2020**, *8*, e9660. [CrossRef]
35. Wang, S.; Wang, Z.; Gao, S.; Zhang, X.; Zeng, J.; Wu, Q. Rare earth elements in lake sediments record historic environmental influences from anthropogenic activities. *Ecol. Indic.* **2024**, *159*, 111680. [CrossRef]
36. Qu, R.; Han, G. Potassium isotopes in herbaceous plants: A potential new tool for C3 and C4 plant research. *J. Geophys. Res. Biogeosci.* **2022**, *127*, e2021JG006682. [CrossRef]
37. Ni, M.; Ma, Y.; Wang, Z.; Wang, X.; Zhu, S. A distinctive mode of dissolved organic carbon biodegradation in karst lakes and reservoirs: Evidence from trophic controls and compositional transformations. *J. Clean. Prod.* **2022**, *368*, 133217. [CrossRef]
38. Zhang, Y.; Li, M.; Du, Y. Distribution of Nitrogen and Phosphorus and Eutrophication Assessment in Water Body of Guanshan Lake Wetland Park. *J. Anhui Agric. Sci.* **2018**, *46*, 60–62. [CrossRef]
39. Yu, X.; Liu, H.; Tian, R.; Lyu, J.; An, Y.; Cheng, P. Using $\delta^{13}C$-$\Delta^{14}C$ to Trace the Source of Dissolved Inorganic Carbon in Reservoirs in the Consolidated Area on the Loess Plateau. *Bull. Mineral. Petrol. Geochem.* **2022**, *41*, 974–980. [CrossRef]
40. Yu, X.; Zhou, W.; Cheng, P.; Wang, Y.; Hou, Y.; Burr, G.S.; Xiong, X.; Wang, Y.; Yang, L.; Dodson, J. Soil organic carbon fractions and ^{14}C ages through 70 years of cropland cultivation. *Soil Tillage Res.* **2019**, *195*, 104415. [CrossRef]

41. Mcnichol, A.P.; Aluwihare, L.I. The power of radiocarbon in biogeochemical studies of the marine carbon cycle: Insights from studies of dissolved and particulate organic carbon (DOC and POC). *Chem. Rev.* **2007**, *107*, 443–466. [CrossRef] [PubMed]
42. Cheng, P.; Burr, G.S.; Zhou, W.; Chen, N.; Hou, Y.; Du, H.; Fu, Y.; Lu, X. The deficiency of organic matter ^{14}C dating in Chinese Loess-paleosol sample. *Quat. Geochronol.* **2020**, *56*, 101051. [CrossRef]
43. Zhong, J.; Wallin, M.; Wang, W.; Li, S.; Guo, L.; Dong, K.; Ellam, R.; Liu, C.; Xu, S. Synchronous evaporation and aquatic primary production in tropical river networks. *Water Res.* **2021**, *200*, 117272. [CrossRef] [PubMed]
44. Shan, S.; Qi, Y.; Luo, C.; Fu, W.; Xue, Y.; Wang, X. Carbon isotopic constrains on the sources and controls of the terrestrial carbon transported in the four large rivers in China. *Adv. Earth Sci.* **2020**, *35*, 948–961.
45. Wen, Z.; Shang, Y.; Lyu, L.; Liu, G.; Hou, J.; He, C.; Shi, Q.; He, D.; Song, K. Sources and composition of riverine dissolved organic matter to marginal seas from mainland China. *J. Hydrol.* **2021**, *603*, 127152. [CrossRef]
46. Liu, H.; Wang, Q.; Yu, X.; Qiu, Z.; Chen, X.; Cheng, P.; An, Y. Analysis of summer DOC in karst reservoirs includes source identification and estimation of input flux. *Acta Sci. Circumst.* **2024**, *44*, 383–392. [CrossRef]
47. Lai, C.; Ma, Z.; Liu, Z.; Sun, H.; Yu, Q.; Xia, F.; He, X.; Bao, Q.; Han, Y.; Liu, X.; et al. Alleviating eutrophication by reducing the abundance of Cyanophyta due to dissolved inorganic carbon fertilization: Insights from Erhai Lake, China. *J. Environ. Sci.* **2023**, *131*, 68–83. [CrossRef]
48. Yin, C.; Zeng, Y.; Chen, J.; Ran, G.; Yang, H.; Yu, J.; Wang, J.; Zhang, Z.; Guo, X. Quantitatively tracing the decomposition of endogenous particulate organic carbon during sinking in (sub-)deep reservoirs: Using radiocarbon isotopes $\Delta^{14}C$. *Water Res.* **2025**, *271*, 123003. [CrossRef] [PubMed]
49. Xiao, J.; Wang, B.; Qiu, X.-L.; Yang, M.; Liu, C.-Q. Interaction between carbon cycling and phytoplankton community succession in hydropower reservoirs: Evidence from stable carbon isotope analysis. *Sci. Total Environ.* **2021**, *774*, 145141. [CrossRef] [PubMed]
50. Jiang, Y.; Lei, J.; Hu, L.; Xiao, Q.; Wang, J.; Zhang, C.; Ali, H. Biogeochemical and physical controls on the evolution of dissolved inorganic carbon (DIC) and $\delta^{13}C_{DIC}$ in karst spring-waters exposed to atmospheric CO_2 (g): Insights from laboratory experiments. *J. Hydrol.* **2020**, *583*, 124294. [CrossRef]
51. Wang, W.; Yi, Y.; Zhong, J.; Kumar, A.; Li, S. Carbon biogeochemical processes in a subtropical karst river–reservoir system. *J. Hydrol.* **2020**, *591*, 125590. [CrossRef]
52. Cai, R.; Jiao, N. Microbial carbon pump shapes chemical signatures of refractory dissolved organic carbon in ocean water column. *Sci. China Earth Sci.* **2024**, *67*, 2408–2410. [CrossRef]
53. Berggren, M.; Guillemette, F.; Bieroza, M.; Buffam, I.; Deininger, A.; Hawkes, J.A.; Kothawala, D.N.; LaBrie, R.; Lapierre, J.F.; Murphy, K.R.; et al. Unified understanding of intrinsic and extrinsic controls of dissolved organic carbon reactivity in aquatic ecosystems. *Ecology* **2022**, *103*, e3763. [CrossRef] [PubMed]
54. Bai, W.Y.; Feng, X.B.; Sun, L.; He, T.; Fu, X.; Jiang, H. The concentration and distribution of mercury in water and sediment porewater of Aha Lake, Guiyang. *Acta Sci. Circumst.* **2006**, *1*, 91–98. [CrossRef] [PubMed]
55. Liu, T.; Zhou, W.; Cheng, P.; Burr, G.S. A survey of the ^{14}C content of dissolved inorganic carbon in Chinese lakes. *Radiocarbon* **2018**, *60*, 705–716. [CrossRef]
56. Wang, J.; Wu, H.; Ao, Q.; Li, Y. Analysis and application of the evaporation of small evaporator and E-601 evaporator based on multiple methods. *J. Mt. Meteorol.* **2024**, *48*, 62–67. [CrossRef]
57. Wu, Y.; Li, M.; Hou, Z.; Ni, Z.; Gao, S.; Li, H.; Wu, H.; Cao, J.; Chu, Z. Long-term trends and rising levels of refractory dissolved organic matter in a suburban plateau lake: Impacts of hydrological changes. *J. Environ. Manag.* **2025**, *386*, 125813. [CrossRef] [PubMed]
58. Parker, S.R.; Poulson, S.R.; Smith, M.G.; Weyer, C.L.; Bates, K.M. Temporal variability in the concentration and stable carbon isotope composition of dissolved inorganic and organic carbon in two Montana, USA rivers. *Aquat. Geochem.* **2010**, *16*, 61–84. [CrossRef]
59. Guo, Y.; Yu, F.; Yang, Y.; Gao, Y.; Shen, M.; Gao, C.; Lv, X.; Wang, D.; Sun, J. Anthropogenic forcing drives centennial-scale phytoplankton productivity dynamics in the East China Sea revealed by biomarker records. *Water Res.* **2025**, *288*, 124547. [CrossRef] [PubMed]

Disclaimer/Publisher's Note: The statements, opinions and data contained in all publications are solely those of the individual author(s) and contributor(s) and not of MDPI and/or the editor(s). MDPI and/or the editor(s) disclaim responsibility for any injury to people or property resulting from any ideas, methods, instructions or products referred to in the content.